Generation of Ribbons, Helicoids and Complex Scherk Surface in Laser-Matter Interactions

Lugomer, Stjepan
Mathematical Research Center for Industrial Technology, Kyushu University | Faculty of Mathematics, Kyushu University

Fukumoto, Yasuhide
Faculty of Mathematics, Kyushu University | Mathematical Research Center for Industrial Technology, Kyushu University

出版情報：MI Preprint Series. 2009-23, 2009-07-16. 九州大学大学院数理学研究院
バージョン：
権利関係：

MI Preprint Series
Kyushu University
The Global COE Program
Math-for-Industry Education & Research Hub

Generation of ribbons, helicoids and complex scherk surface in laser-matter Interactions

S. Lugomer & Y. Fukumoto

MI 2009-23

(Received July 16, 2009)

Faculty of Mathematics
Kyushu University
Fukuoka, JAPAN

Generation of Ribbons, Helicoids and Complex Scherk Surface in Laser-Matter Interactions

S. Lugomer* and Y. Fukumoto†
Faculty of Mathematics and Mathematical Research Center for Industrial Technology, Kyushu University 33, Fukuoka 812-8581, Japan
(Dated: July 16, 2009)

Motivated by a diversity of the shape instability phenomena in condensed matter physics, we study formation of elastic ribbon structures and transformation into helicoidal structures. Using the multi-pulse laser-matter interaction with the Co-coated surface, a one-dimensional high-density vortex filament array has been created. Increasing the number of pulses, the oscillatory strain field causes the cascade of the shape transformations into structures of increasing topological complexity: vortex filaments into ribbons, into ribbon-helicoids and tubular-ribbon-helicoids, and then into short ribbon-structures with the complex Scherk surface being identified. Above a critical number of pulses, the system is catastrophically disintegrated into small-scale wrinkled and crumpled surfaces.

PACS numbers: 47.20.-k, 47.61.-k, 47.80.Jk, 47.32.C-, 46.70.Hg

I. INTRODUCTION

It is well known that nanosecond laser-matter interactions (LMI) may generate a one-dimensional (1D) array of vortex filaments on a solid surface, with the behavior that is common to string-like formations of various systems [1–3]. Among them is the action of torsion that generates the Hasimoto solitons [1], formation and instability of vortex rings [4], the phenomena like helicoidal instability, reconnection, and merging of filaments [2], looping of the filaments in the strain field of a point defect, spiraling and pinning [3] *etc.* All these phenomena are possible due to the fact that vortex filaments (in a certain stage of the LMI), behave as a viscoelastic entity. Their organizational complexity is sensitive on the number of pulses, and various transformation processes into structures of different organizational level of complexity were observed.

From a more general standpoint of the vortex filament dynamics and organization, a question arises as to whether the filaments as 1D string-like formations may transform into 2D ribbon structures. If so, how their behavior varies as the number of pulses is increased? The aim of this study is to provide experimental evidence for the transformation of the filamentary into ribbon-like structures on Co-coated steel. The dependence of this transformation on number of laser pulses is examined.

The melted shear layer of the Co-coated steel behaves, in a certain stage of the nanosecond LMI, like a viscoelastic fluid. Normal stress difference in shearing flows is a fundamental property of viscoelastic fluids [5]. The long ribbons with strongly anisotropic order parameter texture within the vortex sheet are characteristic of the anisotropic fluid mobility, and are consistent with driving oscillatory strain field [5, 6]. We show, in this paper, that the oscillatory strain field which changes in intensity and topology with the number of pulses causes not a single but a cascade of ribbon transformations. As the number of pulses is increased, filamentary objects go through a succession of transformations of vortex micro-filaments into vortex micro-ribbons, into ribbon-helicoids, into ribbon-tube-helicoids, and then into small-scale structures featured by complex Scherk surfaces, and finally, when the number of pulses reaches the critical value, go through their destruction into wrinkled and crumpled surfaces. Once the number of pulses that generate ribbon-helicoid structures reaches the critical value, the organizational scenario to form a more complex structure is exhausted and the system results in destruction of existing structures, being liable to more efficient energy dissipation.

A distinguishing feature of our experiment is the parameterization of the transformation process in terms of the number of pulses and determination of its critical value. A way of dependence on control parameters, such as the chemical-vapor transport rate, the electric field frequency and the mechanical oscillation frequency, is more or less similar to various systems that develop ribbon-type structures. Micro- and nano-ribbons are formed on various materials, such as oxides (ZnO) [7–9], SnO_2 [11–14], biaxial ZnO-Zns [15], ZnS [16], arsenides (GaAs) [17], and selenides (CdSe, ZnSe) [8]. In addition, the semiconductor micro- and nano-ribbons of Si [18], bilayered Si/SiGe, and $NbSe_3$ [19], GaN [20] are produced in a number of experiments, in different interaction environments, of using various substrates. The silicon micro- and nano-ribbons, for example, were produced with thickness 80-100 nm, uniform width 3-5μm and length up to several centimeters in the patterns of very regular structures or very disordered ones [21]. The similar is true of the carbon nano-tube ribbons interpreted as fully collapsed multi-walled carbon nano-tubes as observed in TEM micrographs [21–24]. Many of them appear twisted ribbons

*Electronic address: Stjepan.Lugomer@irb.hr; Permanent addressMaterial Physics Department, Ruder Bošković Institute, Bijenička c.54, 10001 Zagreb, Croatia.
†Electronic address: yasuhide@math.kyushu-u.ac.jp

of about 28-32 nm width, about 478 (approaching 500 nm) length and 470 nm periodic distance between twists, with the torsion angle per unit length $\tau = \pi/470$ nm^{-1} [21]. Many of the stripes of various materials appear to be twisted by angle as large as 180°, with the two ends glued to each other, resulting in a one-sided topology as Möbius stripes, as exemplified by the stripes and belts formed on a compound of niobium and selenium $NbSe_3$ obtained by Tanda *et al.* [19]. The belt diameter and width are typically of 100μm and 1μm, respectively.

Augmenting the list with recently observed structures, it may be said that the ribbons, ribbon helicoids, double helicoidal structures as well as the tubular-ribbon-helicoids span the range from the atomic scale for physical systems like superfluid He [6], the nano-scale for biological systems like peptides [25], DNA molecules [26, 27], polymers [28], various spatial scales of ribbons of other materials, extending up the mega- or astrophysical scale in which they take the form of magnetic-flux ribbons [29] and ribbon flares [30] in the stellar atmospheres.

Despite difference of specific features peculiar to the systems, vortex ribbon structures are of fundamental significance with an unequivocal physical interpretation of the organizational complexity classified at a few hierarchical levels that exhibit some common configuration elements.

II. OUTLINE OF EXPERIMENT

Small samples of Co-coated steel of $1\times1\times0.05$ cm have been exposed to the focused beam of a XeCl ultraviolet laser (wavelength $\lambda = 308$ nm), of energy $E \sim 250-300$ mJ and of the pulse duration $\tau \sim 16-20$ ns, in the open configuration, at low repetition frequency of 2 Hz. The shear layer of melted surface is exposed to acceleration by the shock waves giving rise to the Rayleigh-Taylor (RT) instability with formation of the surface waves and their roll up into micron-scale rolls. The roll-up process is triggered by the parallel scratches (with the scratch-scratch separation distance $L \sim 10$ μm), extending, say, in the x-direction on the target surface. Parallel scratch lines cause the transversal perturbation of the shock wave of the form $A\exp(k_p y)$. Here A is the perturbation amplitude equivalent to the height of the scratch wall, and k_p is the perturbation wavenumber: $k_p = 2\pi/L$ μm^{-1}. An oscillatory shock perturbs the density interface (shear layer) transversally to the radial flow, or the flow from the central to the peripheral regions (y-direction), causing the formation of waves and their roll-up into vortex filaments of the core thickness $\sigma \sim 5-7\mu$m [1–4]. As a result, a high density 1D array of vortex filaments (the separation distance between neighboring filaments $\Lambda \leq \sigma$) has been generated.

The multi-pulse laser irradiation induces oscillatory strain imposed on the vortex-filament array, generating strong lateral compression. Increasing the number of pulses, the strain field becomes inhomogeneous caus-

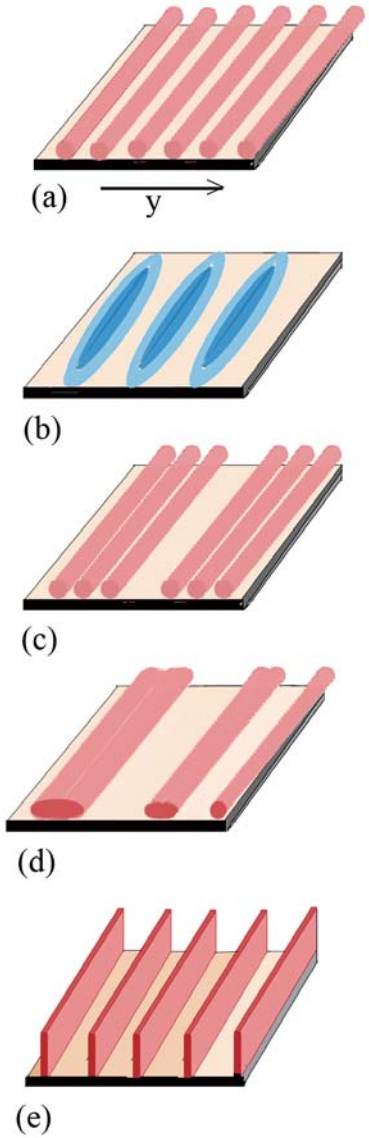

FIG. 1: (Color online). Schematic view of transformation of a 1D vortex-filament array into a 1D ribbon array. (a) A 1D vortex filament array. (b) Oscillatory perturbation generates the stationary wave of the strain field. Dark blue regions designate the region of strong strain field. (c) Grouping of vortex filaments in the regions of weak strain field. (d) Merging of vortex filaments due to lateral compression. (e) A 1D ribbon array.

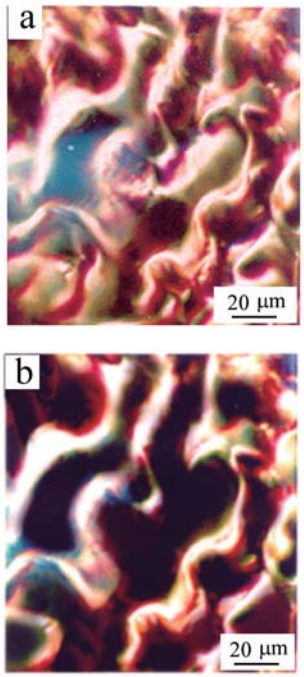

FIG. 2: (Color online) Pattern of the ribbon structures. (a) Optical micrograph of the long and short ribbon structures formed after $N = 17$ pulses. (b) Optical micrograph after numerical filtration and removal of the short structures of (a). The long parallel deformed ribbons are clearly seen.

ing transformation of vortex filaments into more complex structures (Fig. 1). The structures are quenched and stay frozen permanently due to ultrafast cooling after pulse termination, thus making possible *a posteriori* analysis of their micrographs.

III. RESULTS AND DISCUSSION

A. Transformation of vortex filaments into ribbons

Once the filaments are formed after the first few pulses (Fig. 1(a)), the subsequent pulses in a train cause the formation of a strain-wave field oscillation with constant phase (Fig. 1(b)), which brings about almost coherent perturbation, with little modulation, of the filament-array. Exposed to the oscillatory strain field, the filaments come close to each other, becoming grouped in the regions with the minimal strain (Fig. 1(c)). The lateral compression caused by the oscillatory strain induces their axial merging into ribbons (Fig. 1(d)). The longer axes of flattened filaments are parallel to the surface and lie inside the shear layer. The stationary strain wave field drives the ribbons, formed by $N > 10$ pulses, so as to be positioned in the regions of minimal compression (between two maxima), thus generating almost a regular array of ribbons with their surface perpendicular to the substrate, as schematically shown in Fig. 1(e). By increasing the number of pulses, the oscillatory strain field becomes irregular and the ribbon organization becomes complex and disordered. A typical example of almost disordered ribbon array formed after $N = 17$ pulses, is shown in Fig. 2(a). A microscopic analysis reveals an arrangement of long ribbons separated by an empty space, in which the other type of smaller structures is observed. Thus, the pattern indicates two types of underlying dynamics; the primary dynamics which forms the ribbons and the secondary short curved filaments bridging the parallel ribbons. The numerical filtration and elimination of the smaller structures manifests that ribbons of length $L \sim 80-150\mu$m, as the primary structures, are organized into a 1D array with (average) periodicity $\Lambda \sim 25-30\mu$m (Fig. 2(b)). The ribbon width takes $W \sim 15-22\mu$m, and thus their aspect ratio $A = L/W$ ranges from $A \sim 4$ to 10. The refined micrograph in Fig. 2(b) discloses undulation of the ribbons with wavelength $\lambda \sim 15 - 30\mu$m, deformed by development of kinks, dips, and short local helical configurations.

The configuration observed in the micrograph Fig. 3(a)(i) clearly shows that merging of the filaments into a ribbon occurs along their whole length, except at the bended segments whose cores are separated for $\Lambda \sim 20-25\mu$m, *i.e.*, for the distance $\Lambda \gg \sigma$, as schematically shown in Fig. 3(a) (ii). The micrographs in Fig. 3(b) visualize the development of (i) large undulation, (ii) dip, (iii) kink and (iv,v) loop which are all traced to twisting and writhing of the ribbons. This indicates that, at $N = 17$, the inhomogeneous oscillatory strain field already evolves into the micron-scale twisting and writhing domains (strain field point defects), which switches on various types of perturbations of the ribbons.

Description of the observed ribbon configurations can be made in the language of its topological ingredients like the writhe and the twist whose summation is invariant during an inviscid motion [31], though ribbon structure may become involved in time. Define the centerline along the ribbon-tube C by $\boldsymbol{X} = \boldsymbol{X}(s)$, parameterized by the arc-length s along $\boldsymbol{X}$. We attach, to each point on $\boldsymbol{X}(s)$, a segment $\boldsymbol{N}(s)$ of length ϵ, lying on the ribbon surface, normal to the tangent vector to C. We may call the collection of $\boldsymbol{N}(s)$ the director field. Suppose that $\boldsymbol{N}(s)$ is based at $\boldsymbol{X}(s)$. The collection of the end points $\boldsymbol{X}^*(s)$ of $\boldsymbol{N}(s)$ constitute a curve and the linking number L_k of the two curves $\boldsymbol{X}$ and $\boldsymbol{X}^*$, with distance ϵ to each other, serves as a topological invariant of the ribbon. We calculate the twisting angle of the spanwise director field $\boldsymbol{N}$ along $\boldsymbol{X}$. Let $\boldsymbol{t} = \mathrm{d}\boldsymbol{X}/\mathrm{d}s$ be the unit tangent vector along C, $\boldsymbol{n}$ be the unit principal normal and $\boldsymbol{b} = \boldsymbol{t} \times \boldsymbol{n}$ be the unit binormal vectors. Let $\theta(s)$ be the angle of the

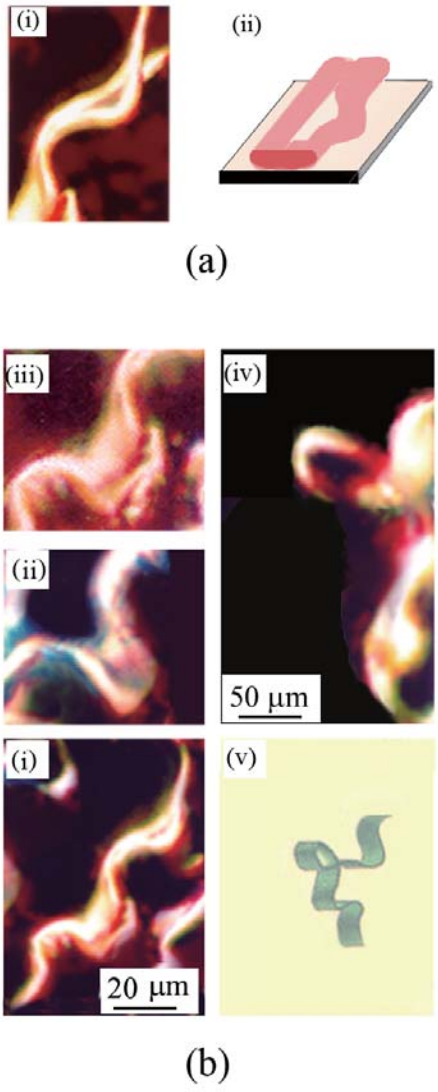

FIG. 3: (Color online) Detail of the ribbon formation by merging of filaments. (a) Vortex filaments merge into ribbons at all places where the filament-filament distance $\Lambda \leq \sigma$ merging does not occur at bended filament segments where $\Lambda > \sigma$. (b) Optical micrograph showing configuration of the ribbon segments: (i) undulation, (ii) dip, (iii) kink, (iv) loop and (v) schematic ribbon-loop reconstruction.

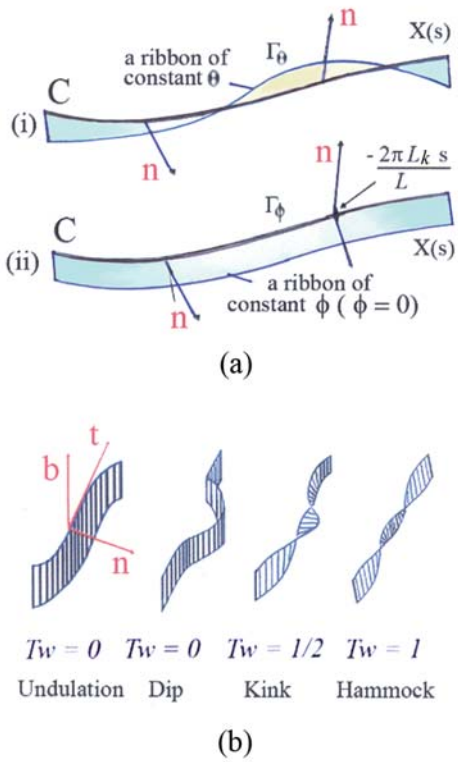

FIG. 4: (Color online) Illustration of the ribbon topology. (a) (i) Ribbon $\theta = \text{const.}$ with boundaries C and Γ_θ which have linking number L_k, (ii) Ribbon $\phi = \text{const.}$ with boundaries C and Γ_ϕ which have zero linking number. (By courtesy of The R. Soc. London, modified Fig. 2 from: A. Y. K. Chui and H.K. Moffatt, Proc. R. Soc. Lond. A **451**, 609 (1995)). (b) Schematic presentation of the ribbon shape instability: undulation, dip, kink and hammock, with the corresponding values of twist T_w, from left to right

spanwise vector relative to $\boldsymbol{n}$. Then $\boldsymbol{N}(s)$ is expressed as

$$\boldsymbol{N}(s) = \epsilon \cos\theta \boldsymbol{n}(s) + \epsilon \sin\theta \boldsymbol{b}(s), \tag{1}$$

In order to have an idea of the twist, we revisit the example a ribbon surface $\theta = \text{const.}$ (Fig. 4(a)) [32]. The ribbon boundary consists of the curve C and the curve Γ_θ of $\theta = \text{const.}$, with distance ϵ to each other. Let L_k be the Gaussian linking number of (C, Γ_θ). We now introduce a new angle variable,

$$\phi = \theta + 2\pi L_k s/L, \tag{2}$$

where L is the total length of C. This choice is called the zero-framing, and has the property that the ribbon of $\phi = \text{const.}$ is *untwisted* in the sense that its boundary curves (C, Γ_ϕ) have zero linking number.

We are now prepared to introduce, for a general ribbon, the total twist T_w, the writhe W_r and their relation to

the linking number L_k [31]. The total twist number of the ribbon is defined by

$$T_w = \frac{1}{2\pi}\oint_C \left(\boldsymbol{N}\times\frac{\mathrm{d}N}{\mathrm{d}s}\right)\cdot\boldsymbol{t}\mathrm{d}s = \frac{1}{2\pi}\oint_C\left(\tau+\frac{\mathrm{d}\theta}{\mathrm{d}s}\right)\mathrm{d}s, \tag{3}$$

The total twist T_w is the sum of the normalized integral of torsion τ of the curve C and of the variation $\mathrm{d}\theta/\mathrm{d}s$ of the angle relative to $\boldsymbol{n}$. The Writhe W_r is defined by

$$W_r = \frac{1}{4\pi}\oint_C\oint_C \frac{(\boldsymbol{X}-\boldsymbol{X}')\cdot(\mathrm{d}\boldsymbol{X}\times\mathrm{d}\boldsymbol{X}')}{|\boldsymbol{X}-\boldsymbol{X}'|^3}. \tag{4}$$

The Călugăreanu theorem states that the Gauss linking number L_k of $\boldsymbol{X}(s)$ and $\boldsymbol{X}^*(s)$, a topological invariant, comprises two parts, the writhe and the twist contribution:

$$L_k = T_w + W_r. \tag{5}$$

The helicity $\mathcal{H}$ is a topological invariant of the continuum; it does not change under continuous deformations. It is tied with the linking number via $\mathcal{H} = \Gamma^2 L_k$, where Γ is the circulation of a bundle of vortex filaments constituting the ribbon [31]. The writhe and the twist, if taken separately, are not topological invariants and their values of T_w and W_r change according to the change of geometry, implying the occurrence of interchange between T_w and W_r during continuous deformation [33].

The writhe W_r is characterized by the following properties: (i) W_r depends only on the geometry of the ribbon-tube axis C, (ii) W_r is invariant under rigid motions or dilations of the space containing C but its sign is changed by reflection. The total twist T_w has the following properties: (i) T_w is a continuous function of C (even through self-intersection), (ii) T_w is invariant under rigid motions or dilations of the space containing the tube, but its sign is changed by reflection, T_w is additive. The total torsion T_w is partitioned into the total torsion and the *intrinsic twist* as displayed in the form of (3). The total twist is a continuous function of C, but the total torsion and the intrinsic twist may be discontinuous in deformations of the tube axis through an inflection point, a point of vanishing curvature [31]. At an inflectional configurations, the twist is abruptly converted into the writhe or *vice versa*. This abrupt conversion of the twist into the writhe could be the origin for the kink instability [33, 34].

Suppose that an open-ribbon is thought of as a large half segment of a ribbon-loop, whose initial helicity is zero [33]. A vortical and shearing boundary motions generate some twisting motion of the ribbon-tube structure of vortices, increasing the twist. This process continues until the critical value for the internal twisting of the field lines is reached, the threshold being determined by the geometry of the ribbon-tube and tension [33, 34]. When the growth of internal twist is no longer tolerated, a further increase in the twist by boundary motions may be converted into the writhe until a force-free equilibrium is reached and, correspondingly, a dip is formed. In a later stage, a further writhing of the flux tube is also impeded and a kink mode instability emerges. In forming a hammock configuration, the vortex ribbon-tube centerline must pass through an inflexional configuration, accompanied by a change in concavity. The conversion of the twist into the writhe is well captured by the following local representation of the ribbon-tube axis $\boldsymbol{X} = (x, y, z)$

$$\begin{aligned} x &= a\cos\xi - cT_w\cos 2\xi, \quad \xi\in[-\pi/2,\pi/2] \\ y &= b\sin\xi - cT_w\sin 2\xi, \quad T_w\in[0,1] \\ z &= cT_w\sin\xi, \end{aligned} \tag{6}$$

where a, b and c are configuration parameters, ξ is a polar angle [33, 34]. The schematic 3D presentation of the ribbon undulation, dip, kink and hammock configurations for $T_w = 0, 1/2, 1$ are shown in Fig. 4(b). It is likely that the instability converting the twist to the writhe is associated with transition to a lower energy state.

Identification of the experimental parameters for the formation of ribbons is, though of importance, limited to be at qualitative level. We found that formation of ribbons does not occur at the low density vortex filament array ($\Lambda \gg \sigma$), but only at the high density one ($\Lambda \leq \sigma$). It means that there exists a critical filament-filament separation distance Λ_c, the corresponding critical wavenumber k_c, and the critical frequency Ω_c of the oscillatory strain field, which enable the formation of ribbons. When these critical parameters are attained, the lateral compression causes the confinement of filaments, moving them into vertical position (one over the other) and then merging them into ribbons (Fig. 1(e)). Namely, compression of the shear layer generates the strain field which is strong in the vertical direction. The strain field requisite for the ribbon formation is the normal strain component developed at the critical oscillatory frequency.

The organization of ribbons into a 1D array is the process that creates the empty space between the ribbons, a kind of a wall defect. In this empty space, the oscillatory excitation causes creation of the new vorticity and the evolution of smaller structures. These secondary structures are separated from the ribbons but may eventually merge with the remnants of the filaments which were not annihilated. They reveal characteristics different from the ribbons, as a result of different local dynamics of the shear layer in the empty space between the ribbons.

The above process of 1D ribbon array formation in multi-pulse LMI is the characteristic of a more general scenario in which vortex filaments experiencing the oscillatory compression, whereby vortex filaments are arranged to form vertical vortex sheets. Becker and Shelly [5] found that an elastic filament embedded in a shear flow yields a normal-stress difference, which are especially large for the oscillating shear. As a consequence, the filament may move no only horizontally but also vertically, out of plane, and change its shape. A local curvilinear flow may exert a driving force of non-Newtonian property like climbing up at the critical shear rate. The origin of such filament behavior lies in the elastic instabilities on

the microscopic scale, occurring when the compressional stresses are sufficiently large as to create large normal-stress differences [5, 6]. A similar effect was observed for the ^{3}He-A superfluid in which the filaments are collected to form vortex stripes and sheets [6]. The formation of stripes, induced by the system rotation, takes place when the rotational frequency reaches the critical frequency. The analogy between the phenomena in LMI and in the superfluid ^{3}He leads us to the speculation that the transition from the filamentary to the ribbon structures is determined by the relaxation rate towards the instantaneous equilibrium. First, the order-parameter texture becomes locally unstable around a nucleation center and the creation of a domain-wall defect follows. When the rotation speed is increased, the new vorticity re-enters in this planar defect, whereby the critical velocity is reduced and the mobility is enhanced. Eltsov *et al.* [6] observed that, in a rapidly oscillating drive, a single sheet becomes unstable and transforms into multiple sheets.

B. Transformation of vortex ribbons into ribbon-helicoids

Increasing the number of pulses to $N = 17 - 20$ causes transformation of a 1D ribbon array into an inhomogeneous pattern of more complex ribbon structures as shown by Fig. 5(a). A numerical filtration and reconstruction of typical structure extracted from the pattern in Fig. 5(a) manifests the screw surface with pitch about 60μm(Fig. 5(b, c)). Another pattern of complex ribbon structures is shown in Fig. 6(a). The most informative structure extracted from the pattern after filtration is displayed in Fig. 6(b). This structure favorably compares with a helicoid, or more precisely with the intermediate structure between a ribbon and a ribbon-helicoid, formed as a consequence of the shape instability. Such an instability occurs when the growing number of pulses induce an oscillatory strain field that executes a strong twisting action on the ribbons. The non-homogeneous twisting action transforms the ribbons into a various kind of helicoids. In addition, the ribbons undergo writhing which causes a number of effects including change in the aspect ratio and formation of kinks. The aspect ratio of a helicoid is defined by $A = h/W$ where W is the length of the rule constituting the surface and h is the pitch of the helicoid [41].

The classical continuum theory for chiral ribbons by Helfrich and Frost [35] rests on the assumption that the ribbon is *isometric*, signifying that it does not support elastic strain [36]. Chiral twist can be imposed on isometric, or non-stretchable, ribbons only by winding them around the surface of a cylinder or a cone, being consistent with the observed spiral ribbon and tube or a set of tubular (rope) structures [36, 37]. On the other hand, if one does allow a ribbon to be stretched but forbids any lateral bending along its axis, then the geometry of the ribbon is restricted to a family of *ruled surfaces*, that is, surfaces generated by the motion of a line [38]. This family includes the helicoid, a twisted minimal surface (Fig. 6(c)) [38].

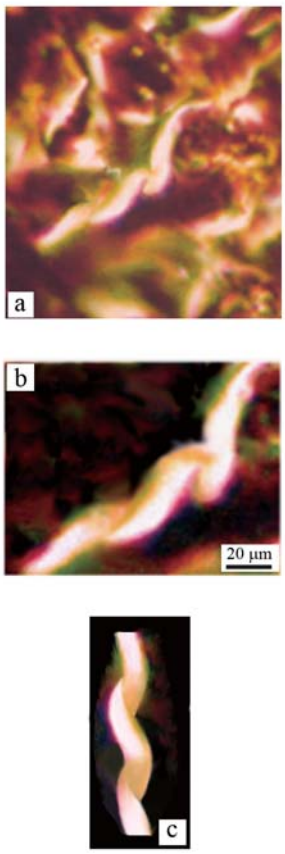

FIG. 5: (Color online) Increasing the number of pulses to $17 < N \leq 20$ causes the shape instability of ribbons. (a) Optical micrograph showing the transformation of the pattern of parallel ribbons into the inhomogeneous pattern of more complex ribbon structures. (b) Micrograph of typical structure extracted from the pattern in (a), by numerical filtration and reconstruction, reveals a screw surface with pitch about 60μm. (c) Reconstruction of the screw structure in (b).

The shape instability which transforms a ribbon into a ribbon-helicoids can be described by a physical model which takes account of finite thickness, elasticity and stiffness. The most appropriate model is the one of Boudaoud *et al.* [41] which describes the formation of a helicoid from the soap film and its instability. For a forced harmonic excitation, the vibration equation of a minimal surface is reduced to the time independent 2D Schrödinger equation. An attractive potential of modified Pöschl-Teller type corresponds to the helicoid, which

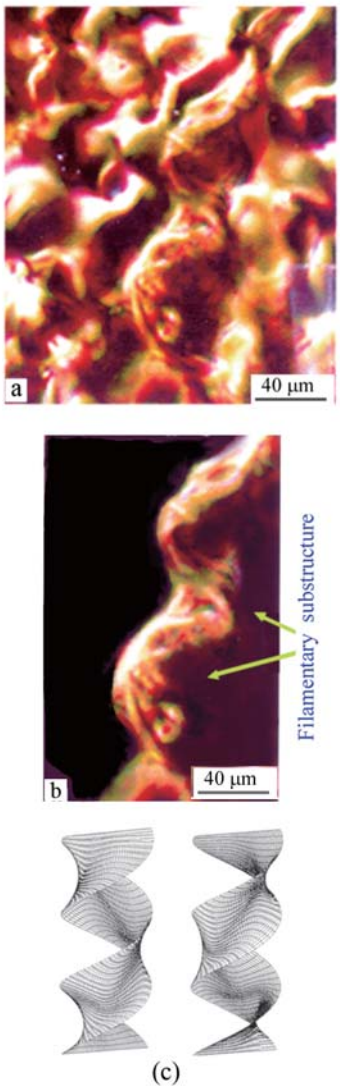

FIG. 6: Complex pattern of ribbon-type structures after the shape transformation. (a) (Color online) Optical micrograph showing the pattern of ribbon-helicoid structures formed at $N = 18$ pulses. (b) (Color online) Ribbon helicoid structure extracted from (a) by numerical filtration. Notice that the ribbon width is increased compared with Fig. 2, the starting one. The refined picture makes visible sub-structure of the ribbon helicoid made up from a collection individual filaments which are not completely merged. (c) Two ribbon-helicoid surfaces obtained by numerical simulation for the aspect ratio $h/W = 2$ and a winding number $\phi_0/\pi = 3$. (Copyright Am. Phys. Society: from A. Boudaoud, P. Patricio and M. Ben Amar, Phys. Rev. Lett. **83**, 3836 (1999)).

admits the eigenfunction to be written in terms of the hypergeometric functions. The construction of a helicoid is shown in Fig. 7. A helicoid under question has height $h = A\phi_0$ and the diameter $W = 2A\sinh\theta_0$, being both fixed, where A is some length parameter. The marginal stability of the helicoid is attained at a critical value of θ_0

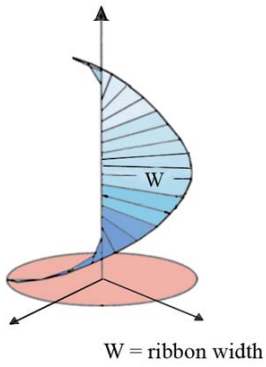

FIG. 7: (Color online) Illustration of the helicoid as a ruled surface formed by the circular motion of a rule.

($\theta_0 > 1.195$), depending on the aspect ratio h/W. When the twist angle ϕ_0 is increased, an instability is switched on, causing destruction of the helicoid and generating a ribbon surface which lies on helices [41].

A close examination of Fig. 6(b) indicates that this structure is not exactly a helicoid, but some transitional (intermediate) structure between the isometric (not elastic) ribbon and the (elastic) helicoid, a continuous transition [41]. The ribbon-helicoid structure in Fig. 6(b) closely resembles the numerically simulated chiral ribbons of Seliger *et al.* [42], who found that they can be obtained by a smooth interpolation between the helicoid and the isometric spiral ribbon with no discernible transition point. This result was obtained by a Monte Carlo simulation of their lattice model for which the ribbon elasticity is characterized by three elastic parameters: $K_{\rm bending}$, $K_{\rm stretching}$ and $K_{\rm twist}$ (or the chiral elastic constant) with $6 \leq K_{\rm stretching} \leq 10$. Accordingly, the ribbon-helicoid structures formed in the multi-pulse LMI possesses significant elasticity which makes possible the formation of surfaces more complex than the ruled surfaces. However, the ribbon elasticity is smaller than that of a single filament. Intuitively, a narrow ribbon is more elastic than a wide ones [42].

Measurement of the width, the thickness, and the length of the ribbons as functions of the number of pulses has shown somewhat different characteristics. The ribbon width increases in a nonlinear way, from $W \sim 18 - 20\mu$m for $N = 17$, to $W \sim 30 - 35\mu$m for $N = 20$, up to almost $W \sim 40\mu$m for $N = 23$ (Fig. 8(a)). The ribbon thickness correspondingly decreases from $d \sim 7\mu$m, to 4.5μm, and finally to 4μm (Fig. 8(b)). This may indicate an opposite behavior from that mentioned by Seliger *et al.* [42]; the elasticity increases with increasing of the width. Another reason for such behavior is inferred from the fact that micrograph reveals 5 vortex filaments in

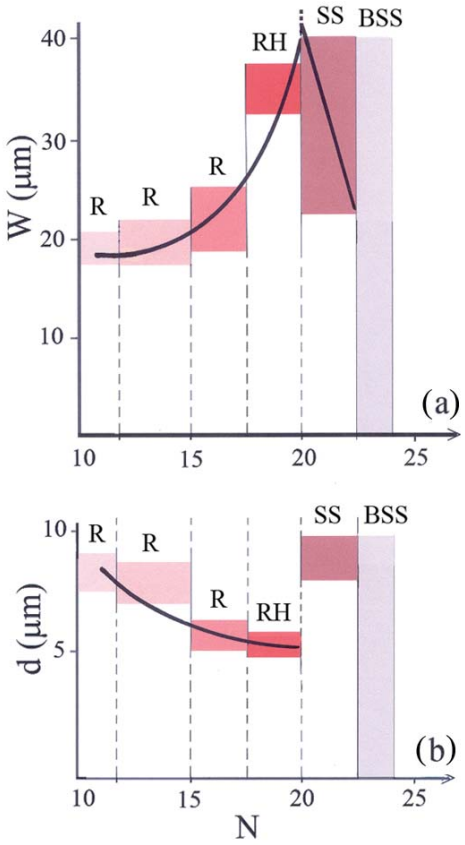

FIG. 8: (Color online) Variation of the ribbon elasticity as a function of the number N of pulses. (a) Diagram showing the nonlinear increase of the ribbon width W with N. The ribbon width gradually grows above $N = 13$, grows faster for $15 \leq N < 17$ and, for $N \geq 17$, drastically increases to the maximum value of $W \geq 40\mu$m, where the breakup of the long ribbon structures into Scherk-surface structures occurs. The breaking the long ribbons into short structures leads to decrease of W. (b) Diagram showing the corresponding nonlinear decay of the ribbon thickness d with N, up to the transition point into the Scherk-surface structures where the ribbon thickness drastically increases. [Legend: R – Ribbon; RH – Ribbon-helicoid; SS –Scherk surface structures; BSS – Breakdown of the Scherk surface structures].

the ribbon structure which are not completely merged (Fig. 6(b)). The increase of the ribbon elasticity in this case originates dominantly from the increase in the gap between neighboring filaments with increasing N.

The helicoids as minimal surfaces are of common occurrence in many soft matter systems ranging from helicoidal organization of lyotropic and thermotropic liquid crystals [43], helicoidal macromolecules, to transformation to ribbons of A-DNA and P-DNA [41]. Examples of intermediate cases between ribbons and helicoids comprising certain elasticity called chiral ribbons are available in biological systems [44].

C. Transformation of vortex ribbons into ribbon-tubular-helicoidal structures

The other type of the ribbon transformation generated at $N = 17 - 20$ is the ribbon-tubular helicoidal structure as shown in Fig. 9(a) with its numerically filtered object Fig. 9(b). This structure could be formed if the ribbon is deformed in such a way that two of its ends start approaching motion rolling around the central axis and are glued together, constituting a tubular surface of circular cross-section (Fig. 9(c)). In the next step, the tube is twisted around the cylinder [45]. Such tubular structures can only be formed when the width W of the ribbon, increasing with the number of pulses, reaches some minimal value necessary for completing the rolling-up motion. The estimation of W from the micrograph Fig. 9(a,b) indicates as wide as 40μm. Such a transformation requires that the elasticity, the bending and the torsional stiffness of the ribbon preserve their integrity. From the mathematical view point, a circular screw surface can be generated by moving a circle under a continuous screw motion. The shape of the surface depends on the orientation of the generating circle. The three types of such surfaces numerically constructed by Havlicek [45] are reproduced in Fig. 9(d). On the right hand side (iii), the plane of the circle which makes helical motion is *horizontal* (orthogonal to the *vertical* axis of the screw). Typical structures of this type were obtained on carbon microcoils by metal catalyzed pyrolisis of acetylene as it can be seen in Fig. 6(b) of Motojima and Chen [22]. In the middle (ii), the plane of the circle is *vertical*. The surface (i) is a screw pipe surface which is the envelope of a sphere subject to a continuous screw motion. In this case the generating circle is neither vertical nor horizontal. Although, at the first glance, these surfaces may look alike but their geometric properties are quite different [45]. The third structure may be identified with the coiling of a filamentary rope around the cylinder and seems to bear resemblance with the structure in Figs. 9(a,b). We remark that this structure is also similar to the magnetic filament rope of Zeldovich *et al.*[46] in dynamo process.

The ribbon-tubular helicoidal structure (Fig. 9(a,b)) as well as the ribbon-helicoid structure (Fig. 6(b)) disclose the existence of fine sub-structures of a bundle of vortex filaments. It is clearly seen that several vortex filaments, though not being completely merged, are twisted in a collective way.

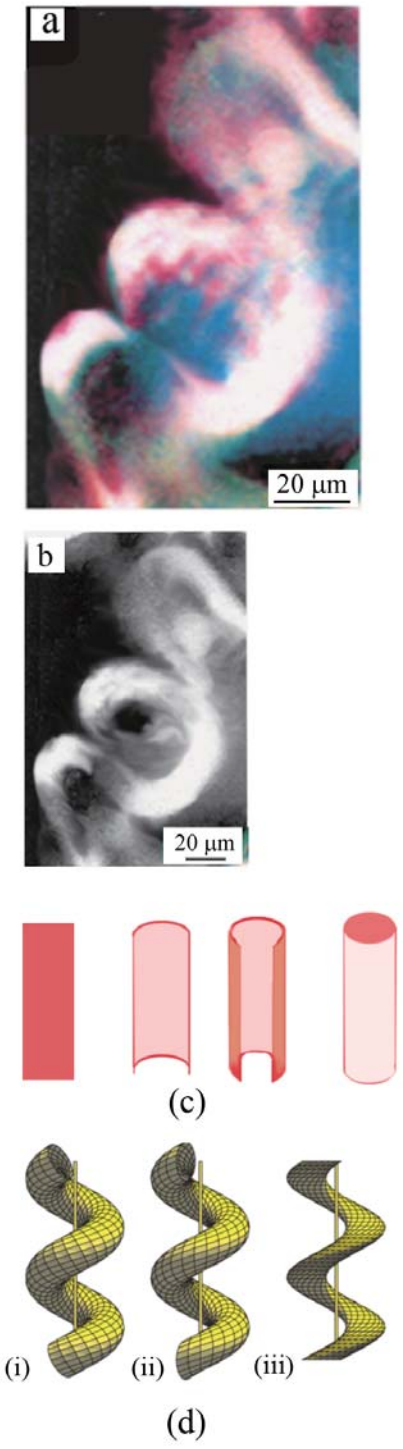

FIG. 9: (Color online) The transformation of a ribbon into a ribbon-tubular-helicoid generated at $17 < N \leq 20$. This type of structure appears if the ribbon is deformed in such a way that it rolls up around the central axis to form a circular cylindrical surface with the two ends glued together. Thereafter the tube is twisted around the cylinder. (a) Optical micrograph of a ribbon-tubular-helicoid. (b) Numerically filtered micrograph from (a). (c) Process of the tubular-ribbon helicoid formation for forming a ribbon-tube of circular cross-section (from left to right), (d) In the next step, the ribbon-tube is twisted around the cylinder giving rise to the tubular-ribbon helicoid, with the following characteristics. (i) The surface is a screw pipe surface which is the envelope of a sphere subject to a continuous screw motion, (ii) the plane of the generating circle is vertical, (iii) the circle is horizontal. (By courtesy of Profs. H. Havlicek and T.U. Wien. From: H. Havlicek, *Advanced Descriptive Geometry*, http://www.geometrie.tuwien.ac.at/havlicek/ergaenz.html)

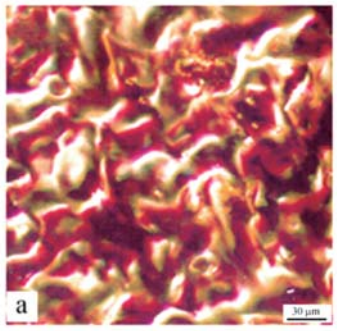

FIG. 10: (Color online) Optical micrograph showing a very complex pattern of the small-scale ribbon structures of the Scherk surface type, formed by the breakdown of the long ribbon-helicoid and tubular-ribbon helicoid structures, above $N = 23$.

D. Break-down of vortex ribbon-helicoids and ribbon-tubular-helicoids: Complex Scherk-surface structures

Increasing the number of pulses to $N = 20 - 23$ causes breakdown of the ribbon-helicoids and ribbon-tubular-helicoids into small-scale structures (Fig. 10). The image filtration and analysis reveal only small fragmented segments with wavy-like surface, the surface with curled edges *etc.* Such catastrophic transformation occurs if the deformation of helicoids and companion tubular structures surpasses their elasticity limit. The growth of strain causes mechanical instabilities of elastic surfaces over a wide range of scales, depending on N as the critical parameter. Typical small-scale structures selected from the complex pattern resemble the complex Scherk surfaces with characteristic edge curling (Fig. 11(a)). Comparison of these surface structures with numerically generated complex Scherk surfaces in Fig. 11(b) exhibits a close similarity. In contrast to a helicoid which has minimal Scherk surface, these structures have the mean curvature $H \neq 0$ [39].

The increase of N to $N > N_{\rm cr}(= 23)$ causes breakdown of the small Scherk surface structures, generating even smaller structures of larger curvature with buckling which become merged into crumpled surfaces. The irregular oscillatory shocks increase the deformation of a surface generating new wrinkles and ridges. Crumpling of an elastic sheet appears to be a highly effective channel for the energy relaxation. As crumpling proceeds with increasing N, the deformation energy tends to concentrate in narrow ridges so that a vicious flow between the structures is induced.

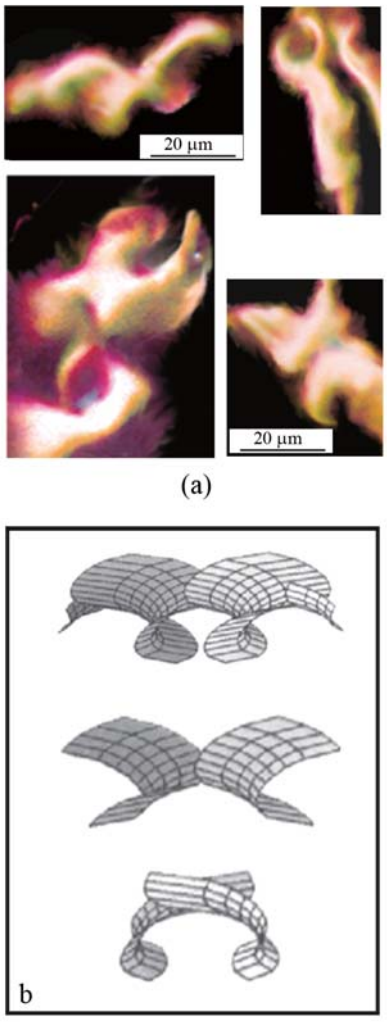

FIG. 11: (Color online) The small-scale Scherk surface structures. (a) Typical structures extracted from the Fig. 10 manifests the characteristics of the complex Scherk surface. (b) The complex Scherk surface structures obtained by numerical simulation. (From: *Le Superfici Minimali*, Capitolo 12; http://www.dm.uniba.it/pertesto/superficie/minimali.doc

Similar small-scale structures which show buckling were found in the pattern of compressed membranes connected with buckling dynamics [47, 48]. Membranes develop wavy patterns whose wavelength grows via coarsening, similarly to rough growing surfaces. The analogy extends even to polymerized membranes formed from equilibrium buckling dynamics of thin elastic sheets in a viscous medium [47]. Furthermore, an analogy is drawn with phenomena of the astrophysical scale as exemplified

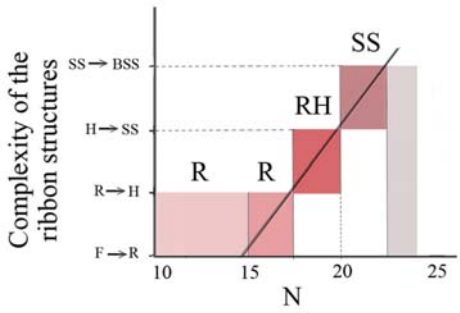

FIG. 12: (Color online) Qualitative diagram showing the complexity of the ribbon structures as a function of N. The complexity increases with N up to $N \geq 23$, when the breakup of the Scherk-surface structures into wrinkled and crumpled structures occurs. [Legend: F → R (Filament into ribbon transition), R → H (Ribbon into ribbon-helicoid transition); H → SS (Helicoid into Scherk surface structure transition), SS → BSS (Breakdown of the Scherk surface structures)]

by the magnetic-field ribbons and ribbon-tubular structures evolving from the magnetic-flux filaments. The magnetic ribbons, helicoids and tubular structures grown by merging close filaments and then exposed to twisting and writhing were studied in connection with the astrophysical dynamo [49, 50]. The electric filament and ribbon structures were generated in a magnetic field driven by the ac electric field. The transition between the structures was induced by variation of the electric field frequency [50]. The oscillatory electric field plays, in the LMI, the role of the oscillatory strain field generated by the series of pulses. Cattaneo's electro-chemical experiment of using oscillating electric field [49] simulates the astrophysical dynamo formation by a multiple parallel arrangement of individual electric-flux filaments, which is responsible for the current amplification [50]. At a critical frequency, the electric ribbons become broken into short deformed segments that resemble the crumpled membrane with fractal surface characteristics.

E. Nonlinear pattern selection and limits of self-organization

The multi-pulse LMI generates structures which are born in the form of vortex filaments and transform into progressively complex structures with increasing the number N of pulses. Starting with the filaments at small N, the ribbons appear in the range $N = 10 - 17$. The increase of N from 17-20 causes the transformation of ribbons into helicoids and ribbon-tubular structures. These

shape transformations represent the switch of the system from an energy relaxational channel into a more efficient one, establishing gradually increasing level of the organizational complexity (Fig. 12). Reaching the ribbon-helicoid and ribbon-tubular state, the system has attained the high level of the organizational complexity. When the number of pulses exceeds $N = 20$, the system cannot develop a more complex pattern organization based on the long ribbons, helicoids and tubes; the elongated structures are disintegrated into short ribbon structures endowed with characteristics of the complex Scherk surfaces. These surfaces represent the limit of self-organizational complexity. Further increase of N beyond $N = 23$ causes violent breakdown of the short ribbon Scherk-surface structures into wrinkled and crumpled surfaces, as the most efficient instantaneous relaxational channel.

IV. CONCLUSION

The multi-pulse laser-matter interaction on the Co-coated steel target surface, endowed with parallel scratches, in the open configuration generates a 1D high-density array of vortex filaments with the periodicity $\Lambda \leq \sigma$. As the number N of pulses is increased, the oscillatory strain field developed in stationary wave field causes the filament grouping and merging into ribbons due to lateral compression. The normal strain component (which is always present under compression) causes the vertical organization of the ribbons with respect to the target surface, and formation of a 1D ribbon array. Further increase of N causes strong perturbation of the array, generating undulations, kinks twists, dips, and other ribbon configurations. At the same time, in the flat fluid space between the ribbons (which in the topological sense represents the quasi 2D wall defect), secondary vortices are created, leading to development of the short-scale structures. The observed ribbon configurations are well described on the basis of their topological properties like the total twist, the writhe and the linking number [31, 34].

The increasing number of pulses causes gradual transformation of vortex ribbons into structures with increasing level of complexity. Two of such structures are identified: ribbon helicoids and ribbon-tube-helicoids. Due to the fact that ribbons have width, thickness, elasticity and stiffness, the new structures are rather the intermediate ones between ribbons and ribbon-helicoids. Such real (physical) structures are well described in a framework developed by Boudaoud *et al.* [41]. Their model describes such structures on the basis of a solution of the time independent Schrödinger equation with an attractive potential wall of so called 'modified Pöschl-Teller' type. Simultaneously with the ribbon-helicoids, the other structures like tubular-ribbon helicoids are observed. According to Havlicek [45], these structures are formed if the ribbon is deformed in such a way that two of its ends start approaching motion around the central axis and meet together to form a cylindrical surface of circular cross-section. As the next step, the tube is twisted around the cylinder. The tubular structures can be formed when the width W of the ribbon exceeds some critical value which makes possible approaching circular motion of both ends of the ribbon. Our estimation is $W > 40\mu$m for occurrence of this rolling-up process of the ribbon. Such transformation requires that the elasticity, bending and stiffness of the ribbon preserve its integrity. As a geometric construction, a circular screw surface can be generated by moving a horizontal circle with a continuous screw motion [45].

Continuing the increase of N causes break-down of ribbon-helicoids and tubular-ribbon-helicoids into short structures. Namely, the enhanced strain causes mechanical instabilities of elastic surfaces. Typical small-scale structures selected from the complex pattern resemble the complex Scherk surfaces with characteristic edge curling. Further increase of N causes, if N goes beyond a certain value, breakdown of the complex Scherk surface structures, generating even smaller structures with buckling, which are merged into crumpled surfaces. The irregular oscillatory shocks increase the deformation of a surface generating new wrinkles and ridges. Crumpling of an elastic sheet provides a highly effective means for the energy relaxation.

Our analysis of complex patterns of ribbon structures on the Co-coated steel strongly indicates that, under oscillatory strain field, the organization of structures changes with increasing N, becoming more complex. This process is caused by tendency of the system to select a configuration suited to more efficient energy relaxation. The process of upgrading organizational complexity with increasing N does not continue indefinitely, owing to some constraints posed by the material integrity. At a critical value of N, the organizational process turns into disintegration of the complex surface structures, thus catastrophically opening a more efficient energy relaxation channel.

Acknowledgments

Our collaboration was supported in part by a Grant-in-Aid for Scientific Research from the Japan Society for the Promotion of Science (No. 21540390). S. L. was also supported in part by the Croatian Ministry of Science, Education and Sport (Project No. 0982915-2899).

[1] Y. Fukumoto and S. Lugomer, Phys. Lett. A **308**, 375 (2003).

[2] S. Lugomer, Phys. Lett. A **361**, 87 (2007).

[3] S. Lugomer, Y. Fukumoto, B. Farkas, T. Szörényi and A. Toth, Phys. Rev. E **76**, 016305 (2007).
[4] S. Lugomer and Y. Fukumoto, Fluid Dyn. Res. **36**, 277 (2005).
[5] L. E. Becker and M. J. Shelley, Phys. Rev. Lett. **87**, 198301 (2001).
[6] V. B. Eltsov, R. Blauwgeers, N. B. Kopnin, M. Krusius, J. J. Ruohio, R. Schanen and E. V. Thuneberg, Phys. Rev. Lett. **88**, 065301 (2002).
[7] B. A. Korgel, Science **303**, 1308 (2004).
[8] Z. L. Wang, X. Y. Kong and Y. Ding, Microsc. Microanal. **10** (Suppl. 2), 528 (2004).
[9] Z. W. Pan, Z. R. Dai and Z. L. Wang, Science **291**, 1947 (2001).
[10] Z. R. Dai, Z. W. Pan and Z. L. Wang, Solid State Commun. **118**, 351 (2001).
[11] M. W. Murphy, P. S. G. Kim, X. Zhou, J. Zhou, M. Coulliard, G. A. Botton and T. K. Shaw, J. Phys. Chem. C **113**, 4755 (2009).
[12] C. Borchers, D. Stichtenath, S. Muller, D. Schwen and C. Ronning, Nanotechnology **17**, 1067 (2005).
[13] S. McKernan, G. J. Zhou and B. Carter, Phil. Mag. Lett. **64**, 1362 (1991).
[14] L. Yang, X. Zhang, R. H. Zhang and X. An, Solid State Commun. **130**, 769 (2004).
[15] T. Hanrath and B. A. Korgel, Adv. Mater. **3**, 1625 (2003).
[16] D. D. Hou, Y. K. Liu, J. A. Zapien, Y. Y. Shan and S. T. Lee, Optoelectronic Lett. **4**, 161 (2008).
[17] H. C. Ko, A. J. Baca and J. A. Rogers, Nano Lett. **6**, 2318 (2006).
[18] W. Shi, H. Peng, N. Wang, C. P. Li, L. Xu, C. S. Lee, R. Kalish and S.-T. Lee, J. Am. Chem. Soc. **123**, 11095 (2001).
[19] S. Tanda, T. Tsuneta, K. Yamaya and N. Hatakanaka, Nature **417**, 397 (2002).
[20] S. Biswas, S. Kar, T. Ghoshai, V. D. Ashok, S. Chakrabarti and S. Chaudri, Mat. Res. Bull. **42**, 428 (2007).
[21] M.-F. Yu, M. J. Dyer, J. Chen, D. Qian, W. Liu and R. S. Ruoff, Phys. Rev. B **64**, 241403 (2001).
[22] S. Motojima and X. Chen, Bull. Chem Soc. Jpn. **80**, 449 (2007).
[23] R. Gao, Z. L. Wang and S. Fan, J. Phys. Chem. B **104**, 1227 (2000).
[24] A. Szabo, A. Fonsca, J. B. Nagy, Ph. Lambin and L. P. Biro, Carbon **43**, 1628 (2005).
[25] G. Ballesia, M. V. Fedorov and E. G. Timoshenko, J. Chem. Phys. **128**, 195105 (2008).
[26] T. Strick, J.-F. Allemand, D. Bensimon, R. Lavery and V. Croquette, Physica A **263**, 392 (1999).
[27] M. D. F. Kamenetskii, J. Mol. Str.(Theochem) **336**, 235 (1995).
[28] S. Koombhongse, W. Liu and D. H. Reneker, J. Polym. Sci. Part B: Polym. Phys. **39**, 2598 (2001).
[29] W. Xie, H. Zhang and H. Wang, Solar Phys. **254**, 271 (2008).
[30] C. Liu, J. Lee, D. E. Gary and H. Wang, Astrophys. J. **658**, L127 (2007).
[31] H. K. Moffatt and R. L. Ricca, Proc. R. Soc. London A **439**, 411 (1992).
[32] A. Y. K. Chui and H. K. Moffatt, Proc. R. Soc. London A **451**, 609 (1995).
[33] R. L. Ricca, paper in VII European Meeting on *Solar Physics*, Catania, Italy (ed. G. Belvedere, 1994) p. 151.
[34] R. L. Ricca, Fluid Dyn. Res. **36**, 319 (2005).
[35] W. Helfrich and J. Prost, Phys. Rev. A **38**, 3065 (1988).
[36] R. Gafourui and R. Bruinsma, Phys. Rev. Lett. **94**, 138101 (2005).
[37] Zhao, S. Zhang, Z. Yao and L. Zhang, Phys. Rev. E **74**, 032801 (2006).
[38] R. Osserman, *A Survey of Minimal Surfaces*, (Dover Pubns, 1986).
[39] A. Fogden and S. T. Hyde, Eur. Phys. J. B **7**, 91 (1999).
[40] Capitolo 12, Le Superfici Minimali, http://www.dm.uniba.it/pertesto/superficie/minimali.doc
[41] A. Boudaoud, P. Patricio and M. Ben Amar, Phys. Rev. Lett. **83**, 3836 (1999).
[42] R. L. B. Selinger, J. V. Selinger, A. P. Malanoski and J. M. Schnur, Phys. Rev. Lett. **93**, 158103 (2004).
[43] R. D. Kamien and T. C. Lubensky, Phys. Rev. Lett. **82**, 2892 (1999).
[44] C. Branden and T. Tooze, *Introduction to Protein Structure*, (Garland Publishing Inc., New York, 1991).
[45] H. Havlicek, http://www.geometrie.tuwien.ac.at/havlicek /ergaenz.html
[46] Ya. B. Zeldovich, A. A. Ruzmaikin and D. D. Sokoloff, *The Almighty Chance*, (World Scientific, Singapore, 1990) p. 215.
[47] D. Moldovan and L. Golubovic, Phys. Rev. Lett. **82**, 2884 (1999).
[48] J. A. Astrom, J. Timonen and M. Karttunen, Phys. Rev. Lett. **93**, 244301 (2004).
[49] F. Cattaneo, *Astrophysical Dynamo Action*, ppt (2004).
[50] M. Mukerjee, Sci. Am. **Jan.** (1995).

List of MI Preprint Series, Kyushu University

The Global COE Program
Math-for-Industry Education & Research Hub

MI

MI2008-1 Takahiro ITO, Shuichi INOKUCHI & Yoshihiro MIZOGUCHI
Abstract collision systems simulated by cellular automata

MI2008-2 Eiji ONODERA
The intial value problem for a third-order dispersive flow into compact almost Hermitian manifolds

MI2008-3 Hiroaki KIDO
On isosceles sets in the 4-dimensional Euclidean space

MI2008-4 Hirofumi NOTSU
Numerical computations of cavity flow problems by a pressure stabilized characteristic-curve finite element scheme

MI2008-5 Yoshiyasu OZEKI
Torsion points of abelian varieties with values in nfinite extensions over a p-adic field

MI2008-6 Yoshiyuki TOMIYAMA
Lifting Galois representations over arbitrary number fields

MI2008-7 Takehiro HIROTSU & Setsuo TANIGUCHI
The random walk model revisited

MI2008-8 Silvia GANDY, Masaaki KANNO, Hirokazu ANAI & Kazuhiro YOKOYAMA
Optimizing a particular real root of a polynomial by a special cylindrical algebraic decomposition

MI2008-9 Kazufumi KIMOTO, Sho MATSUMOTO & Masato WAKAYAMA
Alpha-determinant cyclic modules and Jacobi polynomials

MI2008-10 Sangyeol LEE & Hiroki MASUDA
Jarque-Bera Normality Test for the Driving Lévy Process of a Discretely Observed Univariate SDE

MI2008-11 Hiroyuki CHIHARA & Eiji ONODERA
A third order dispersive flow for closed curves into almost Hermitian manifolds

MI2008-12 Takehiko KINOSHITA, Kouji HASHIMOTO and Mitsuhiro T. NAKAO
On the L^2 a priori error estimates to the finite element solution of elliptic problems with singular adjoint operator

MI2008-13 Jacques FARAUT and Masato WAKAYAMA
Hermitian symmetric spaces of tube type and multivariate Meixner-Pollaczek polynomials

MI2008-14 Takashi NAKAMURA
Riemann zeta-values, Euler polynomials and the best constant of Sobolev inequality

MI2008-15 Takashi NAKAMURA
Some topics related to Hurwitz-Lerch zeta functions

MI2009-1 Yasuhide FUKUMOTO
Global time evolution of viscous vortex rings

MI2009-2 Hidetoshi MATSUI & Sadanori KONISHI
Regularized functional regression modeling for functional response and predictors

MI2009-3 Hidetoshi MATSUI & Sadanori KONISHI
Variable selection for functional regression model via the L_1 regularization

MI2009-4 Shuichi KAWANO & Sadanori KONISHI
Nonlinear logistic discrimination via regularized Gaussian basis expansions

MI2009-5 Toshiro HIRANOUCHI & Yuichiro TAGUCHII
Flat modules and Groebner bases over truncated discrete valuation rings

MI2009-6 Kenji KAJIWARA & Yasuhiro OHTA
Bilinearization and Casorati determinant solutions to non-autonomous 1+1 dimensional discrete soliton equations

MI2009-7 Yoshiyuki KAGEI
Asymptotic behavior of solutions of the compressible Navier-Stokes equation around the plane Couette flow

MI2009-8 Shohei TATEISHI, Hidetoshi MATSUI & Sadanori KONISHI
Nonlinear regression modeling via the lasso-type regularization

MI2009-9 Takeshi TAKAISHI & Masato KIMURA
Phase field model for mode III crack growth in two dimensional elasticity

MI2009-10 Shingo SAITO
Generalisation of Mack's formula for claims reserving with arbitrary exponents for the variance assumption

MI2009-11 Kenji KAJIWARA, Masanobu KANEKO, Atsushi NOBE & Teruhisa TSUDA
Ultradiscretization of a solvable two-dimensional chaotic map associated with the Hesse cubic curve

MI2009-12 Tetsu MASUDA
Hypergeometric τ-functions of the q-Painlevé system of type $E_8^{(1)}$

MI2009-13 Hidenao IWANE, Hitoshi YANAMI, Hirokazu ANAI & Kazuhiro YOKOYAMA
A Practical Implementation of a Symbolic-Numeric Cylindrical Algebraic Decomposition for Quantifier Elimination

MI2009-14 Yasunori MAEKAWA
On Gaussian decay estimates of solutions to some linear elliptic equations and its applications

MI2009-15 Yuya ISHIHARA & Yoshiyuki KAGEI
Large time behavior of the semigroup on L^p spaces associated with the linearized compressible Navier-Stokes equation in a cylindrical domain

MI2009-16 Chikashi ARITA, Atsuo KUNIBA, Kazumitsu SAKAI & Tsuyoshi SAWABE
Spectrum in multi-species asymmetric simple exclusion process on a ring

MI2009-17 Masato WAKAYAMA & Keitaro YAMAMOTO
Non-linear algebraic differential equations satisfied by certain family of elliptic functions

MI2009-18 Me Me NAING & Yasuhide FUKUMOTO
Local Instability of an Elliptical Flow Subjected to a Coriolis Force

MI2009-19 Mitsunori KAYANO & Sadanori KONISHI
Sparse functional principal component analysis via regularized basis expansions and its application

MI2009-20 Shuichi KAWANO & Sadanori KONISHI
Semi-supervised logistic discrimination via regularized Gaussian basis expansions

MI2009-21 Hiroshi YOSHIDA, Yoshihiro MIWA & Masanobu KANEKO
Elliptic curves and Fibonacci numbers arising from Lindenmayer system with symbolic computations

MI2009-22 Eiji ONODERA
A remark on the global existence of a third order dispersive flow into locally Hermitian symmetric spaces

MI2009-23 Stjepan LUGOMER & Yasuhide FUKUMOTO
Generation of ribbons, helicoids and complex scherk surface in laser-matter Interactions